

Signatures of granular microstructure in dense shear flows

Daniel M. Muehle¹, Georges F. Debregeas¹, Greg S. Karacmar², Peter J. Eng³,
Sidney R. Nagel¹, and Heinrich M. Jaeger¹

¹The James Franck Institute and Department of Physics, The University of Chicago,
5640 S. Ellis Avenue, Chicago, IL 60637

²Radiology Department, The University of Chicago

³Center for Advanced Radiation Sources (CARS), The University of Chicago

45.70.-n,05.40.-a,45.70.Cc,81.05.Rm

Granular materials react to shear stresses differently than do ordinary fluids. Rather than deforming uniformly, materials such as dry sand or cohesionless powders develop shear bands: narrow zones containing large relative particle motion leaving adjacent regions essentially rigid [1,5]. Since shear bands mark areas of flow, material failure and energy dissipation, they play a crucial role for many industrial, civil engineering and geophysical processes [6]. They also appear in related contexts, such as in lubricating fluids confined to ultra-thin molecular layers [7]. Detailed information on motion within a shear band in a three-dimensional geometry, including the degree of particle rotation and inter-particle slip, is lacking. Similarly, only little is known about how properties of the individual grains—their microstructure—affect movement in densely packed material [5]. Combining magnetic resonance imaging, x-ray tomography, and high-speed video particle tracking, we obtain the local steady-state particle velocity, rotation and packing density for shear flow in a three-dimensional Couette geometry. We find that key characteristics of the granular microstructure determine the shape of the velocity profile.

In order to probe the role of microstructure inside the narrow granular shear zone, independent determinations of the velocity and density profiles with spatial resolution well below the size of individual particles are required. Non-invasive measurements of this type so far have been limited to two-dimensional (2D) geometries where optical tracking of all particle positions is straightforward [2,4,8,11]. In a 3D Couette cell, as sketched in Fig. 1a, a steady-state shear flow can be set up by confining granular material between two concentric, vertical cylinders and turning the inner cylinder at constant velocity v_{wall} while keeping the outer wall at rest. Unlike 2D Couette cells [9,10], where particles are confined to a single layer with constant volume, there is a free upper surface allowing the packing density to adjust via feedback between shear-induced dilation and gravity.

The difficulty of imaging the interior has restricted studies of 3D granular Couette systems to either probing only the surface [12], to tracking colored tracers in very narrow (few particles wide) cells [13], or to measuring

global quantities, such as the total applied torque and its fluctuations [12]. Here we use magnetic resonance imaging (MRI) to obtain flow velocities from the interior of a 3D system [14,15]. We have used oil-rich seeds as a source of free protons that can be traced using MRI [14]. Two kinds of seeds were used to explore the role of microstructure: mustard seeds (spherical with mean diameter $d = 1.8\text{mm}$) and poppy seeds (kidney-shaped with mean diameter $d = 0.8\text{mm}$). The wall friction was controlled by gluing a layer of seeds on both cylinders. Using a spin-tagging technique, horizontal slices were imaged, as sketched in Fig. 1a. In the resulting MRI image (Fig. 1b), the shear band shows up as the narrow region of deformed stripes near the inner, moving, cylinder. Imaging slices at different heights, h , we measured these deformations from which the azimuthal velocity profiles were calculated throughout the cell. Similarly, three-dimensional x-ray tomography allowed us to calculate packing fraction profiles at various heights (Fig. 1d). At the transparent cell bottom additional velocity and packing fraction information was gathered by direct, high-speed-video particle tracking (Fig. 1c).

Prior to each set of measurements, the cell was run until steady-state was reached (as determined by the fact that the packing density profiles became stationary). Over a total acquisition time of typically 17min per MRI slice, high-resolution images revealed the long-time average local displacements during a time interval, $t = 100\text{ms}$ (Fig. 1b). The azimuthal velocity at a given distance r from the inner wall was obtained by exploiting the cylindrical symmetry of the Couette geometry: we calculated the MRI intensities along a circle of radius r , $I_{\text{turning}}(\theta)$ and $I_{\text{stopped}}(\theta)$, for the cell turning and at rest, respectively. The position of the central peak in the cross-correlation between $I_{\text{turning}}(\theta)$ and $I_{\text{stopped}}(\theta)$ corresponds to the average azimuthal distance traveled by the material during t . This technique yielded the angle- and time-averaged radial profile of the steady-state azimuthal mass flow velocity, $v(r)$, resolving $v(r)$ to within 0.1mm/s and r to within 0.1mm . Note that this high-resolution mass flow velocity is the average velocity of all material at radius r and thus not only contains information about particle translation and spin, but also depends on packing fraction. This differs from the average velocity of particle centers that typically is obtained by video particle tracking techniques.

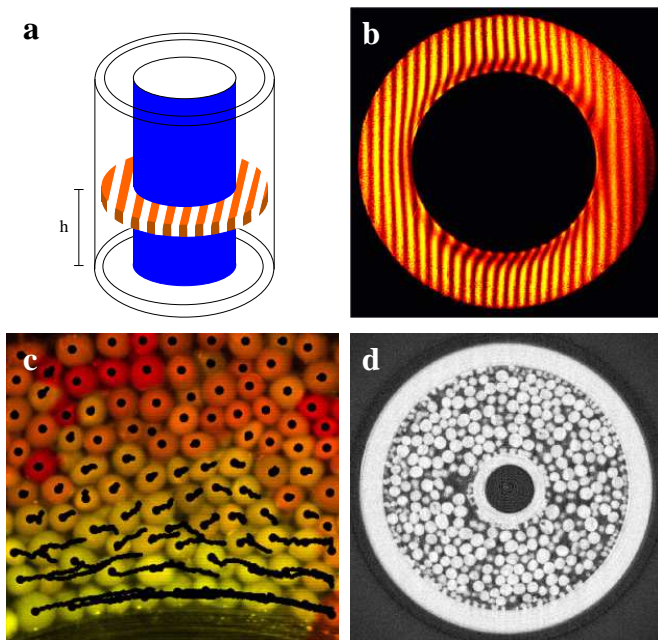


FIG. 1. Non-invasive MRI, x-ray tomography and high-speed video probes of granular Couette flow. (a) Sketch of the Couette-type shear cell consisting of two concentric cylinders with diameters 51mm and 82mm and filled to a level of 60mm. The inner cylinder was rotated at angular velocities from 0.6-45rpm, corresponding to $0.6\text{mm/s} < v_{\text{wall}} < 120\text{mm/s}$. The flow velocity was measured using a MRI spin-tagging technique [14,15]. Before imaging, proton spins were encoded (spin-tagged) so as to display parallel stripes when imaged. Images were taken of 5mm thick horizontal slices at various heights, h . (b) When the inner cylinder was rotated, distortion of the stripe pattern revealed the displacement of the material that occurred during the 100ms interval between spin-tagging and imaging. 2048 spin-tag-image steps were used to assemble each complete image. (c) High-speed video frame, taken at 1/1000s, of mustard seeds observed through the cell's transparent bottom. To indicate the movement history of individual particles, their center positions over the preceding 200 frames are traced by black lines. The particle coloring reflects the magnitude of each particle's average velocity during this 0.2s interval: fast particles (yellow) near the inner wall appear to move smoothly, while slower particles (orange and red) display more irregular and intermittent motion. In the long-time average, measured by the MRI technique, the flow appears smooth everywhere. (d) Two-dimensional, horizontal slice through the cell at half the filling height, taken from x-ray tomography data set. Particles, in this case mustard seeds, appear bright (as do the walls of the cell). These measurements were performed at the Advanced Photon Source at Argonne National Lab in a Couette cell of slightly smaller size but under otherwise identical shearing conditions.

We found $v(r)$ highly reproducible from run to run even though on shorter time scales there are rapid velocity fluctuations from point to point within the material that, at the boundaries, can be observed with high-speed video (Fig. 1c) [16]. Within the resolution of our measurements, $v(r)$ for both types of seeds did not vary with height, including the regions near the top and bottom surfaces (Note that this indicates that non-azimuthal, secondary flow was small and did not affect $v(r)$, in accordance with tracer-bead studies [13]). Aside from an overall scale factor, we also did not detect any shear-rate dependence to the velocity profile over the entire range $5\text{mm/s} < v_{\text{wall}} < 120\text{mm/s}$ explored with MRI. (With video imaging we verified rate independence down to velocities as small as 0.6 mm/s) [16].

For (nearly) monodisperse smooth, spherical particles, the decay of $v(r)$ away from the shearing wall is dominated by abrupt drops at integer multiples of $r=d$ as shown in Fig. 2a for mustard seeds. In the normalized velocity gradient $(r) \frac{d \langle v \rangle}{v \langle r \rangle}$ (Fig. 2b) these drops appear as deep narrow valleys. They are correlated with pronounced oscillations in the packing density, (r) , which signal the presence of well-defined, single-grain-wide layers near the moving wall (Fig. 2c). (We note that the average density approaches the random close packing value at larger r in a manner that is consistent with an exponential form [10].) The shear-induced layering is reminiscent of that seen [17] in the collisional regime of dilute flows, but occurs here in the high-density limit of rate-independent, frictional flow. Since the velocity drops are highly localized, we associate them with slipping at the interface between adjacent layers. Either directly from $v(r)$ or by comparing the integrated areas of each valley in (r) we find that across each slip zone the velocity decreases by approximately the same factor, $b = 0.36 \pm 0.13$.

In addition to slip between layers, MRI resolves a non-zero velocity gradient (r) within each layer. This can be caused by either particle rotation or disorder in the layering along the radial direction. (Along the azimuthal and axial directions, particles within layers certainly show packing disorder as can be seen from the maximum in (r) in Figs. 2c and 3c whose values lie significantly below those for a crystalline configuration). For perfectly arranged layers, (r) at the layer centers would be determined solely by particle rotation (spin) within each layer. The presence of particles which do not lie perfectly within the layers (revealed by the non-zero values of (r) between layers in Fig. 2c and seen directly from the tracks in Fig. 1c) reduces the gradient in the slip region and increases it at the layer centers. In the limit of complete disorder, we would expect the staircase shape of $v(r)$ to vanish completely. Using information about the density, (r) , and velocity, $v_c(r)$, of the particle centers, as determined by the high-speed video and x-ray experiments, we find that approximately 90% of (r) at the layer centers is due to the radial disorder. In order for the MRI and high-speed video experiments to give the same (r) , particle spin must be considered, revealing the spin pro-

As seen in the inset of Fig. 2a. We note that the spin is small, increasing slowly with distance from the shearing wall to a value at $r=d = 4.5$ of less than one full particle rotation per $13d$ translation.

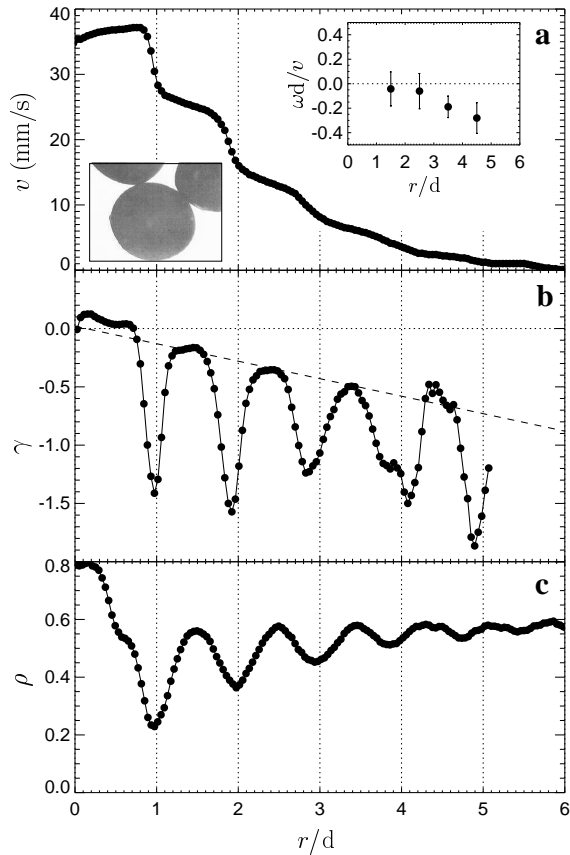


FIG. 2. Radial velocity, spin and packing density profiles for spherical mustard seeds. (a) Steady-state, angle-averaged azimuthal velocity $v(r)$ across the shear band at $h = 30\text{mm}$, halfway below the filling level. The layer of seeds glued to the inner cylinder wall extends to the dotted vertical line at $r=d = 1$. The lower inset shows a photograph of the seeds. The upper inset shows the normalized particle spin rate, $\omega d/v$, as a function of distance from the moving wall (where ω is the angular velocity of a particle about its center). (b) Normalized velocity gradient $\gamma = (d=v)/v = \partial v/\partial r$ for the data in the main panel of (a). (c) Angle-averaged, steady-state radial packing density profile $\rho(r)$ computed from x-ray tomography data as in Fig. 1d, measuring the volume fraction occupied by seed material. For $0 < r=d < 1$ the seeds glued to the wall contribute to ρ .

The message of Fig. 2 is that the overall shape of $v(r)$ across the shear band can be understood as arising from two main contributions to the velocity gradient $\dot{\gamma}(r)$: a slip contribution in the presence of layering, and a second contribution associated with radial disorder. These two pieces are distinguished by the characteristic r -dependence they produce in $v(r)$ on length scales larger

than a single grain. A constant slipping fraction,

$$\int_{\text{interface}} \dot{\gamma}_{\text{slip}}(r) dr = b;$$

across each interface, by itself, leads to a velocity profile with an exponential decay, $v(r) = v_0 \exp(-br/d)$. The constant inter-layer slip appears on a background due to radial disorder, $\dot{\gamma}_{\text{disorder}}(r) = 2c(r - r_0)/d$, that starts at r_0 within the glued-on layer and increases linearly in strength with slope $2c$ as indicated by the dotted line (Fig. 2b). Such linear r -dependence in $\dot{\gamma}(r)$ results in a Gaussian profile, $v(r) = v \exp[-c(r-d - r_0/d)^2]$. The sum of the two contributions to $\dot{\gamma}(r)$, after integration, leads to a product of an exponential and Gaussian term for the overall, averaged velocity profile:

$$v(r) = v_0 \exp\left[-b \frac{r}{d} - c \frac{(r - r_0)^2}{d^2}\right]$$

Fits of this function to mustard seed data yield $b = 0.36 \pm 0.13$, $c = 0.06 \pm 0.03$ and $r_0/d = 0.6 \pm 0.8$ independent of height and shear rate.

The decomposition of $\dot{\gamma}(r)$ allows the quantitative tracking of the slip inside the shear band for different particle types. We find a greatly reduced slip rate b when smooth spherical particles are replaced by roughened ones [16]. More dramatic differences result from changes in the particle shape. For kidney-shaped poppy seeds we observe a comparatively smooth overall velocity profile (Fig. 3a). Much smaller modulations in $\dot{\gamma}(r)$ (Fig. 3b) together with little layering in $\rho(r)$ (Fig. 3c) indicate that interlayer slip is greatly reduced. The linear trend $\dot{\gamma}(r) = 2c(r-d - r_0/d)$ is still present, however, and leads to the Gaussian shape for $v(r)$ seen in Fig. 4 over several orders of magnitude. These data also demonstrate explicitly that the shear rate fixed by $\dot{\gamma}_{\text{wall}}$, while setting the overall scale, leaves the shape of the profile unchanged. This allows for a collapse of all poppy seed data for different shear rates and heights in the cell onto a single Gaussian described by $c = 0.11 \pm 0.02$ and $r_0/d = 0.1 \pm 0.5$. Layering can also be suppressed and radial disorder promoted in sphere packings if wide particle size distributions are used. We find that these, too, produce essentially Gaussian velocity profiles [16].

From these results, the Gaussian component of the velocity profile emerges as a robust, generic feature; slip, if it occurs, is seen to augment $v(r)$ by an additional, exponential factor. In contrast to the translationally invariant slip, the explicit dependence of the Gaussian on the distance from the shearing wall indicates correlations. There are several possible mechanisms for radial correlations [5,9,10,18,20], including the formation of stress chains [5,9,10] or particle clusters [18,20], both of which require high packing densities and the absence of slip or some degree of interlocking. However, a detailed mechanism that would explain the observed Gaussian dependence presently does not exist. A successful theory must

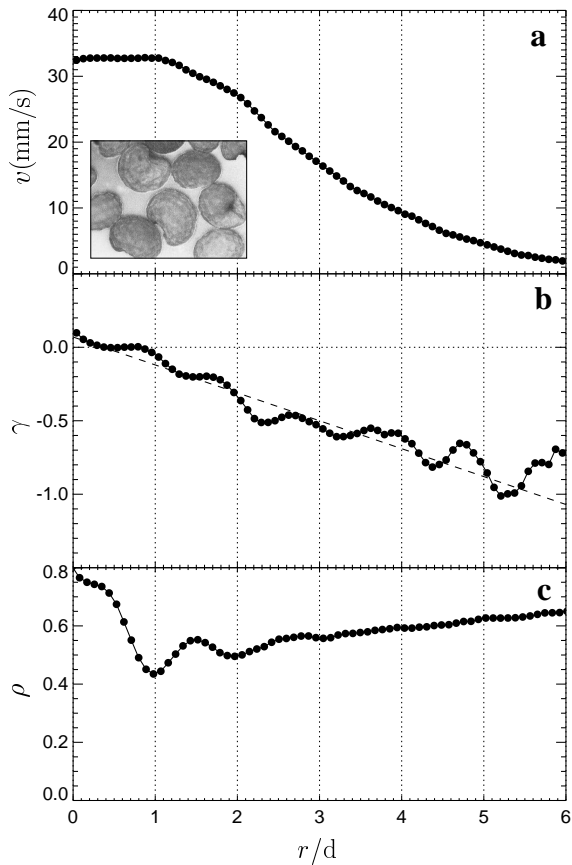


FIG. 3. Radial velocity, spin and packing density profiles for aspherical poppy seeds. (a) Steady-state, angle-averaged azimuthal velocity $v(r)$ across the shear band at $h = 30$ mm. The inset shows a photograph of the seeds. (b) Normalized velocity gradient for the data in (a). (c) Corresponding angle-averaged, radial packing density profile $\rho(r)$ from x-ray data. For $0 < r=d < 1$ the seeds glued to the wall contribute to

not only account for the linear increase in the magnitude of the velocity gradient with r , but also show how the Gaussian shape is independent of the presence of layering. We speculate that both of these might be provided by a coupling of $\rho(r)$ to the average packing fraction and its gradients (for 2-D Couette systems a coupling to the average density alone has been suggested [9,10]). A Gaussian, then, arises naturally for a coupling of type $\rho(r) / \rho(r_0) \sim \exp(-r/r_0)$, considering first order terms in r . Because all stress-loading is driven by the seed layer glued to the inner wall, its location, r_0 , serves as a spatial reference point. This argument carries over to the absence of a Gaussian contribution to $v(r)$ in less dense types of flow, where interlocking may be less effective, such as rapid flows down inclines with free upper surface for which power law forms have been reported [4,14,21], or vertical gravity-driven flows through 2D "pipes", which appear to follow essentially exponential profiles [2,22].

Our results show that in this high packing density and

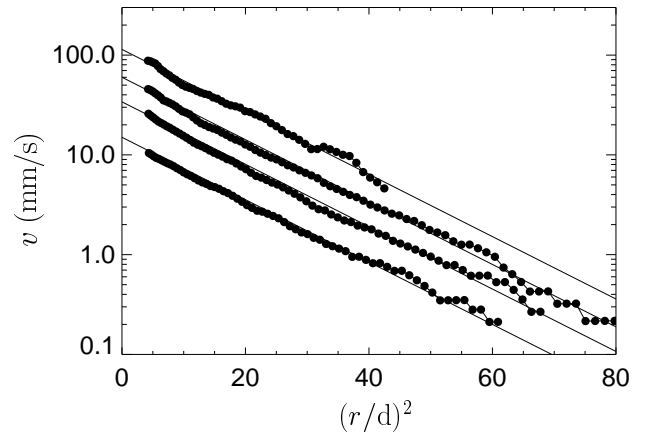


FIG. 4. Rate-independence of the velocity profiles. Log plot of poppy seed velocity profiles $v(r)$ as a function of $(r=d)^2$ for four different shearing wall speeds ($v_{\text{wall}} = 120, 52, 33,$ and 14 m/s, top to bottom). Straight lines on this plot correspond to a Gaussian with origin at $r = 0$. The slope, c , of these lines corresponds to half the average slope of the velocity gradient in Fig. 3b and characterizes the width $l = d = c$ of the shear band.

slow shearing rate regime there is a direct connection between the microstructure and the shape of the velocity profile. For equal-sized spherical particles, where considerable layering is found, a strong exponential contribution is observed. For aspherical seeds, which show no pronounced layering, the profile is almost completely described by a Gaussian centered on the shearing wall. Remarkably, despite the complicated nature of the grain-grain interactions, the steady-state behavior exhibits robust behavior: the shape of the velocity profiles characterized by the two length scales, $l = d = b$ and $l = d = c$, is found to be height and shear-rate independent.

ACKNOWLEDGMENTS

We thank Eiichi Fukushima, James Jenkins, Christophe Josserand, Dov Levine, Milica Medved, Vachantang Putkaradze, Mark Rivers, and Alexei Tkachenko for helpful discussion, and Doris Stockwell from Spiceland for the donation of mustard seeds for the experiment. This work was supported by an NFS research grant and by the MRSEC Program of the NSF.

-
- [1] J. Bridgwater. On the width of failure zones. *Geotechnique* 30, 533 (1980).
 - [2] R. M. Neddeman and C. Laohakul. The Thickness of the Shear Zone of Flowing Granular Materials. *Powder Technology* 25, 91-100 (1980).

- [3] H. B. Muhlhau and I. Vardoulakis. The thickness of shear bands in granular materials. *Geotechnique* 37, 271-283 (1987).
- [4] T. G. Drake. Structural Features in Granular Flows. *Journal of Geophysical Research* 95, 8681-8696 (1990).
- [5] M. Oda and H. Kazama. Microstructure of shear bands and its relation to the mechanism of dilatancy and failure of dense granular material. *Geotechnique* 48, 465-481 (1998).
- [6] D. R. Scott. Seismicity and stress rotation in a granular model of the brittle crust. *Nature* 381, 592-595 (1996).
- [7] S. G. Rannick. Soft Matter in a Tight Spot. *Physics Today* 52, 26-31 (1999).
- [8] U. Tuzun and R. M. Neddeman. An Investigation of the Flow Boundary During Steady-State Discharge from a Funnel-Flow Bunker. *Powder Technology* 31, 27-43 (1982).
- [9] D. Howell, R. P. Behringer and C. Veje. Stress Fluctuations in a 2D Granular Couette Experiment: A Continuous Transition. *Physical Review Letters* 82, 5241-5244 (1999).
- [10] C. T. Veje, D. W. Howell and R. P. Behringer. Kinematics of a two-dimensional granular Couette experiment at the transition to shearing. *Physical Review E* 59, 739-745 (1999).
- [11] J. Rajchenbach. Granular flows. *Advances in Physics* 49, 229-256 (2000).
- [12] W. Losert and J. P. Gollub. Flow properties of granular matter fluidized by gas or shear. *Bull. Am. Phys. Soc.* 44, 47 (1999).
- [13] R. Khosropour, J. Zirinsky, H. K. Pak and R. P. Behringer. Convection and size segregation in a Couette flow of granular material. *Physical Review E* 56, 4467-4473 (1997).
- [14] E. Fukushima. Nuclear Magnetic Resonance as a Tool to Study Flow. *Annu. Rev. Fluid Mech.* 31, 95-123 (1999).
- [15] E. E. Ehrichs, H. M. Jaeger, G. S. Karczm ar, J. B. Knight, V. Y. Kupernan and S. R. Nagel. Granular Convection Observed by Magnetic Resonance Imaging. *Science* 267, 1632-1634 (1995).
- [16] D. M. M ueth, G. F. D ebregeas, P. J. Eng, G. S. K arczm ar, S. R. N agel and H. M. Jaeger. to be published.
- [17] M. A. Hopkins, J. T. Jenkins and M. Y. Louge. On the Structure of Three-Dimensional Shear Flows. *Mechanics of Materials* 16, 179-188 (1993).
- [18] G. D ebregeas and C. Josserand. A self-similar model for shear flows in dense granular material. cond-m at 9901336 (preprint).
- [19] A. Tkachenko and V. Putkaradze. Mesoscopic physics of granular flows. cond-m at/9912187 (preprint).
- [20] C. Josserand. A 2D asymmetric exclusion model for granular flows. *Europhysics Letters* 48, 36-42 (1999).
- [21] D. M. Hanes and D. L. Inman. Observations of rapidly flowing granular-fluid materials. *Journal of Fluid Mechanics* 150, 357-380 (1985).
- [22] O. Pouliquen and R. Gutfraund. Stress Fluctuations and Shear Zones in Quasi-Static Granular Chute Flows. *Physical Review E* 53, 557-561 (1996).